Dalton Transactions

ROYAL SOCIETY OF CHEMISTRY

PAPER

View Article Online
View Journal | View Issue

Check for updates

Cite this: *Dalton Trans.*, 2023, **52**, 10206

pH-driven optical changes of platinum(II) complexes having carboxy-appended salophen ligands†

Shun Fujii,[a] Hajime Yagi,[a,b] Tomohiro Kawaguchi,[a] Mitsuru Ishikawa,[a,b] Naoki Izumiyama[a] and Manabu Nakaya *[a,b]

Received 29th March 2023,
Accepted 3rd July 2023

DOI: 10.1039/d3dt00956d

rsc.li/dalton

Platinum(II) complexes with salophen ligands bearing carboxy substituents at different positions, [Pt{(COOH)$_n$–salophen}] (n = 2 (**1**), 3 (**2**), 1 (**3**)), were synthesized and characterized by acquiring UV-vis and luminescence spectra. These complexes exhibited systematic variations in absorption spectra depending on the number of carboxy groups, and this effect was attributed to metal–ligand charge transfer with support from density functional theory calculations. The luminescence properties of these complexes were also correlated with structural differences. Complexes **1–3** showed systematic spectral changes by addition of organic acid and base, respectively. This is based on the protonation/deprotonation of the carboxy substituents. Furthermore, aggregation-induced spectra change was investigated in DMSO–H_2O mixtures with various proportions of water. Peak shifts in the range of 95 to 105 nm occurred in the absorption spectra in conjunction with pH changes. These variations resulted from molecular aggregation and diffusion associated with protonation/deprotonation of the carboxy groups. Variations in luminescence emission intensity and peak shifts were also observed. This work provides new insights into the correlations between the optical properties of carboxy-appended molecular complexes and pH changes and will assist in the future design of pH sensing devices based on molecular metal complexes.

Introduction

Metal complexes exhibiting luminescent properties, such as those based on platinum(II), iridium(III) and ruthenium(II), have been intensively investigated with regard to potential applications in optical devices,[1–3] biological imaging,[4–7] photo-sensitizers,[8–10] chemical sensing[11–15] and light-emitting diodes.[16–19] The effects of molecular arrangements, organic substituents (that is, ligand modification) and external stimuli (including heat, pressure and pH) on the luminescent properties of these compounds have also been evaluated.[20–22] Knowledge of the relationship between optical properties and external stimuli is especially important when developing chemical sensing devices. On this basis, various metal complexes exhibiting tuneable luminescence properties have been reported. Above all, from the perspective of environmental application, metal complexes exhibiting photo-functions based on variations in molecular assembly triggered by protonation and deprotonation in conjunction with pH changes have been widely investigated.[23–25] These pH-responsive luminescent complexes tend to contain hydroxy groups and/or N atoms acting as Lewis bases that can readily accept protons. Among these chemically-responsive metal complexes, square-planar d8 platinum(II) complexes show promise as external-stimuli-responsive luminescent molecules because the electronic states of these complexes vary with molecular structure. Cyclometalated platinum(II) complexes have been designed that incorporate N^N^C, N^C^N or C^N^C tridentate ligands in which the C or N atoms serve as coordinating donor atoms. As well, Schiff-base platinum(II) complexes having tetradentate ligands with N_2O_4 or N_4 moieties have been reported.[26–30]

The present work investigated the effect of protonation/deprotonation of carboxy groups on the optical properties of platinum(II) complexes incorporating salophen ligands with carboxy groups, [Pt{(COOH)$_n$–salophen}] (n = 2 (**1**), 3 (**2**), 1 (**3**)) (Scheme 1), and demonstrated the pH-dependent spectroscopic changes of the complexes.

These complexes were synthesized using a previously reported procedure with minor modifications (see the Experimental section and ESI†).[31] Each complex was initially

[a]*Department of Material Science, Graduate School of Science, Josai University, 1-1 Keyakidai, Sakado, Saitama 350-0295, Japan. E-mail: nakaya@josai.ac.jp*
[b]*Department of Chemistry, Faculty of Science, Josai University, 1-1 Keyakidai, Sakado, Saitama 350-0295, Japan*

†Electronic supplementary information (ESI) available. CCDC 2251726 2251727. For ESI and crystallographic data in CIF or other electronic format see DOI: https://doi.org/10.1039/d3dt00956d

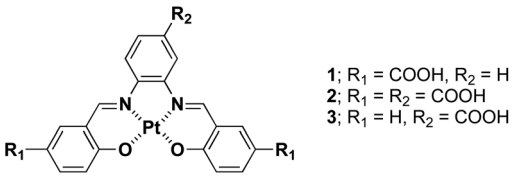

1; R_1 = COOH, R_2 = H
2; R_1 = R_2 = COOH
3; R_1 = H, R_2 = COOH

Scheme 1 Molecular structures of complexes **1–3**.

isolated as its potassium salt as a consequence of deprotonation of the carboxy groups during the synthesis process. These salts were dissolved in water after which the addition of 2 M HCl precipitated the target compounds **1–3** as dark orange solids. These materials were characterized by ^{1}H-NMR, single crystal X-ray diffraction (SC-XRD), elemental analysis and mass spectrometry. The optical properties of each complex under various conditions were also investigated along with the structural feature.

Results and discussion

Crystal structures

Single crystals of complexes **1** and **3** suitable for SC-XRD analysis were obtained *via* the slow evaporation of solutions of these complexes in DMSO–MeOH mixtures over several days. SC-XRD data acquired from complex **1** at 100 K showed that this compound crystalized in the monoclinic space group $P2_1/c$ (Fig. 1a). The crystal parameters are summarized in Table S1.† Complex **1** was also found to contain a DMSO solvent in the crystal lattice. The two carboxy groups in this complex were evidently protonated because there was no evidence of counter cations. In the molecular assembly, a short contact indicating a Pt···Pt interaction was observed and the Pt···Pt distance was determined to be 3.253 Å (Fig. 1b). The data showed that a pair of **1** molecules interacted with a neighbouring molecule *via* hydrogen bonding involving the carboxy groups, with an intermolecular distance of approximately 1.89 Å. Within the crystal packing, molecules of **1** formed a one-dimensional assembly along the *a* axis that incorporated DMSO molecules (Fig. 1c). In contrast to the monoclinic space group of **1**, complex **3** at 100 K crystalized in the trigonal space group $P\bar{3}c1$ (Fig. 2a). The crystal parameters for this complex are also provided in Table S1.† Complex **3** was found to have a plane of symmetry but was distorted, as indicated by the side-view in Fig. 2a. In addition, the data showed that water molecules were included in the crystal lattice of **3**. The crystal packing structure of this complex exhibited one-dimensional channels along the *c* axis (Fig. 2b and c). The carboxy groups evidently did not undergo dimerization based on hydrogen bond formation but were oriented in the direction of the channel pores. These groups would therefore be expected to promote the capture of water molecules in the channels *via* hydrogen bonding. Unfortunately, a single crystal of complex **2** suitable for SC-XRD analysis could not be obtained.

UV-vis and luminescence spectra

Each complex was poorly soluble in many organic solvents because of the carboxy substituents but would dissolve in polar nonprotic solvents such as DMF, DMSO and THF. Therefore, spectroscopic measurements were conducted using DMSO as the solvent. Fig. 3 shows the UV-vis spectra (dashed lines) and normalized luminescence spectra (solid lines) obtained from complexes **1–3** in DMSO. Complexes **1** and **2** each produced an absorption peak at 505 nm based on the metal-to-ligand charge transfer (MLCT) that is typical of Schiff-base-type Pt(II) complexes.[28] In contrast, complex **3** generated a peak related to MLCT that was slightly red-shifted to 535 nm. This difference can possibly be attributed to the reduced repulsive effect of the negatively-charged deprotonated carboxy groups in the case of **3**. In addition, the oligomer was formed in the molecular assemblies through the wide π-plane in the ligand. Although omitted here to simplify the figure, strong

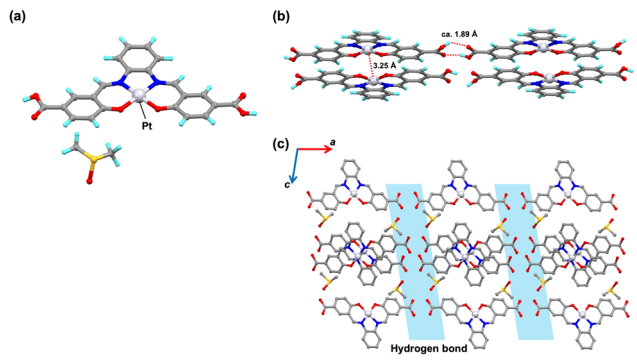

Fig. 1 (a) The crystal structure of **1**. Color code: C, grey; N, blue; H, light blue; O, red; Pt, white. (b) A representation of intermolecular hydrogen bonding and Pt···Pt interactions between molecules of **1**. (c) The molecular assembly of **1** in the *ac* plane. Hydrogen atoms are omitted for clarity.

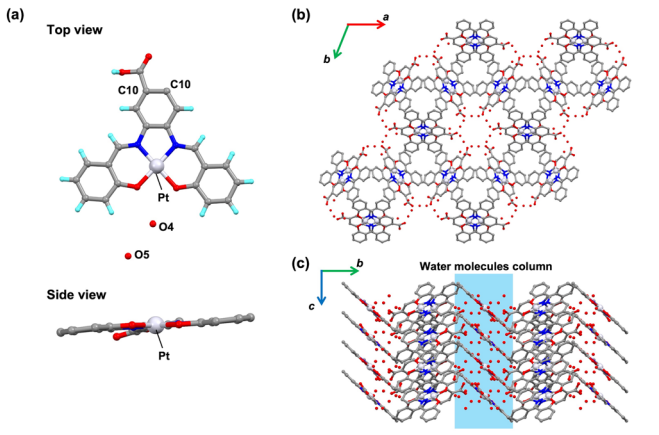

Fig. 2 (a) Crystal structure of **3**. The top view shows the entire molecule while the side view presents the distorted structure. Color code: C, grey; N, blue; H, light blue; O, red; Pt, white. Molecular assembly of **2** in (b) the *ab* plane and (c) the *bc* plane. Hydrogen atoms are omitted for clarity.

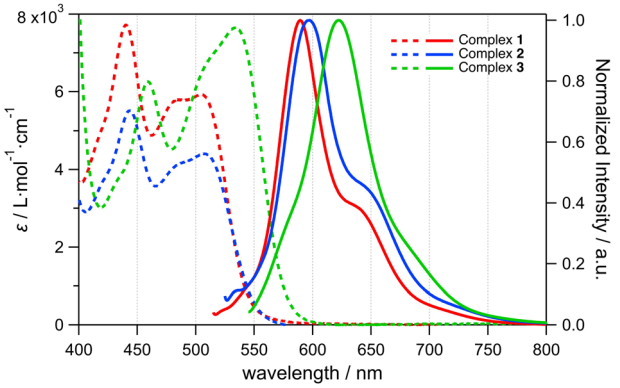

Fig. 3 UV-vis spectra (dashed lines) and luminescence spectra (solid lines) obtained from complexes **1–3** at 20 μM in DMSO at 25 °C.

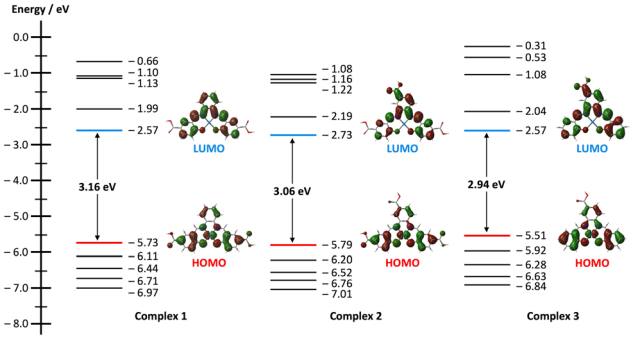

Fig. 4 An energy diagram showing the frontier orbitals and energy values for **1** (left), **2** (middle) and **3** (right) calculated at the B3LYP/LANL2DZ/6-31G* theoretical level.

adsorption bands assigned to intra-ligand charge transfer (ILCT) were observed below 400 nm. The luminescence spectra of **1** and **2** each exhibited a peak around 590 nm while the same peak for **3** was red-shifted to 620 nm. The emission quantum yields (QYs, φ_{em}) of **1–3** was obtained at room temperature. The QYs of **1** (φ_{em} = 0.003) and **2** (φ_{em} = 0.001) were relatively determined based on the QYs obtained in DMSO–H_2O mixture (see later session, Table 2). QYs of **3** was φ_{em} = 0.04.

DFT calculations

To obtain an improved understanding of the absorption spectra of **1**, **2** and **3**, density functional theory (DFT) and time-dependent DFT (TDDFT) calculations at the B3LYP[32] theoretical level were performed using the Gaussian 16 program[33] with the basis sets LANL2DZ for Pt atom and 6-31G (d) for all other atoms. In all calculations, the solvent effects of DMSO were included by conductor-like polarizable continuum model (CPCM). The geometric parameters of **1** were optimised based on the solid-state structure obtained from the SC-XRD analysis. The structures of **2** and **3** were then optimised based on the structure of **1**. These optimized structures were verified by vibrational frequency calculations (they have no imaginary vibrational frequency). The HOMO and LUMO of all three complexes and the associated energy levels are displayed in Fig. 4. In each case, the HOMO was evidently distributed over the Pt (II) centre and the salophen ligands, including the carboxy substituents. However, the carboxy groups introduced to the upper phenyl ring (part of the phenylenediamine moiety) in **2** and **3** had little effect on the electron density distribution. Consequently, the HOMO energy level of **2** was similar to that of **1** while the HOMO energy level of **3** was slightly higher than those of **1** and **2**. The LUMO in each complex was distributed on a π-conjugated salophen ligand core. Because a HOMO → LUMO transition was involved in the $S_0 \rightarrow S_1$ transition, the absorption peaks of **1–3** that appeared in the range of 500–550 nm were assigned to MLCT phenomena. Complex **1** also generated MLCT/ILCT bands involving $S_0 \rightarrow S_2$ and $S_0 \rightarrow S_3$ transitions that were primarily attributed to HOMO–1 → LUMO and HOMO → LUMO+1 transitions (predicted to occur in the range of 400–421 nm). The results of calculations for complexes **2** and **3** were very similar to those obtained for **1**, such that all the absorption bands could be assigned to MLCT or ILCT transitions. Details regarding the transitions for complexes **1–3** are provided in Fig. S1–S3 and Table S2.†

Titration experiments with acid and base

Because the carboxy groups could be protonated or deprotonated based on the acid and base addition, titration experiments of **1–3** with suitable acid and base were performed. Complex **1** was titrated with potassium *tert*-butoxide (*t*-BuOK; base) from 0 to 14 equivalents of base, which was monitored by luminescence spectra changes (Fig. 5). Deprotonation of **1** resulted in slightly red-shift of the $\lambda_{em\ max}$ and gave an increase of emission intensity (Fig. 5a, top). The peak shift was almost completed by the addition of 4 eq. of base, however, the emission intensity kept increasing until the addition of 14 equivalents of base. This is because the deprotonation was completed and then further addition of base induced ionic interaction between carboxylate and potassium cation, causing the interference with heat inactivation and the aggregation-induced emission enhancement (AIEE). Following the titration with base, further titration of the basic solution was performed

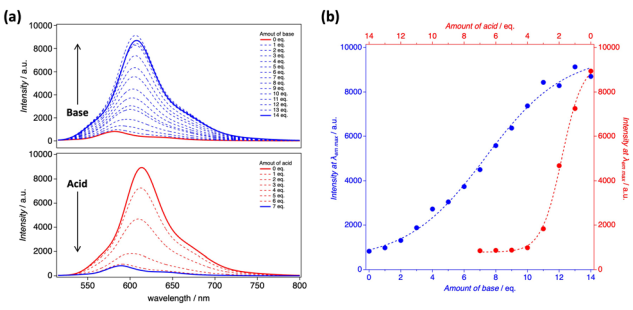

Fig. 5 (a) Luminescence spectra of **1** (20 μM in DMSO at 25 °C) while titrating with (top) *t*-BuOK from 0 to 14 eq. and (bottom) TsOH from 0 to 7 eq. (b) Titration plots of intensity changes at $\lambda_{em\ max}$ of **1**. Blue and red plots indicate the titration by base and acid, respectively.

with *p*-toluenesulfonic acid (TsOH; acid) from 0 to 7 equivalents of acid (Fig. 5a, bottom). The emission intensity enhanced by base addition was drastically decreased by just addition of 4 eq. of acid, *i.e.*, the elimination of AIEE phenomena was induced by the re-protonation of the carboxylate site by the appropriate amount of acid (Fig. 5b). Therefore, this acid/base titration resulted in proving the reversibility of the protonation/deprotonation in **1**. In both acid and base titration, **1** were found to show sigmoidal spectra change, in which the protonatioin/deprotonation phenomena occurred cooperatively. In complexes **2** and **3**, appropriate acid and base likewise induced the reversibility in the luminescence spectra (Fig. S4 and S5†). The spectral change (red- or blue-shift) of **1–3** induced by the deprotonation was also corroborated by DFT calculation (Table S3†). The energy value of the $S_0 \rightarrow S_1$ transition of **1** was found to decrease by deprotonation (ex. 2.53 eV → 2.41 eV), which supports the red-shift of emission spectra. Similar calculated data was obtained in complex **2**. As for complex **3**, the deprotonation resulted in blue-shift of the emission spectra, which is also supported by the DFT calculation. In all the simulation, the oscillator strength did not changed between the protonated and deprotonated Pt(II) complexes. In other words, the intensity change attributed to the molecular aggregation.

pH dependence in aggregation induced spectra change

As studied above, acid and base obviously induced emission changes based on protonation/deprotonation in the present Pt (II) complexes. Next, molecular aggregation which frequently affects the luminescence property of Pt(II) complexes were investigated with various pH water. All data were acquired in mixtures of DMSO with water, the pH of which had been adjusted to 2.0, 6.4 or 13.0. In these experiments, the concentration of each Pt(II) complex was fixed at 20 μM and the proportion of water in the solvent was changed from 0% to 90%.

Fig. 6a–c present the UV spectra of complex **1** as generated with various water proportions and at different pH condition. At a pH of 2, **1** was less soluble in water and so may have preferentially migrated to the DMSO as good solvent. Therefore, upon increasing the proportion of water to 40%, the peak at approximately 504 nm gradually became less intense and then underwent a remarkable decrease in association with the formation of a precipitate (Fig. 6a). At a pH of 6.4, a similar peak decrease was observed but the decrease occurred sequentially, not drastically, because **1** was slightly soluble in water at this pH condition. Conversely, at a pH of 13.0, the carboxy substituent of **1** was deprotonated. In this case, even with a 10% proportion of water, the complex molecules were soluble in the basic water sites working as good solvent, resulting in a large red-shift from 505 to 600 nm in the UV-vis spectrum. Despite the absorption maximum was red-shifted by 95 nm at max at basic condition, the emission spectra was hardly shifted (mentioned later). Therefore, the peak shift of the adsorption spectra is originated from the formation of oligomer based on the pH change. With increases in the water proportion, the peak was gradually blue-shifted down to 495 nm. This occurred because the negatively-charged carboxylate moieties accelerated the complex molecules to repel each other in the solution so as to inhibit the oligomer formation. Table 1 summarizes the peak shifts of **1** at different pH together with the

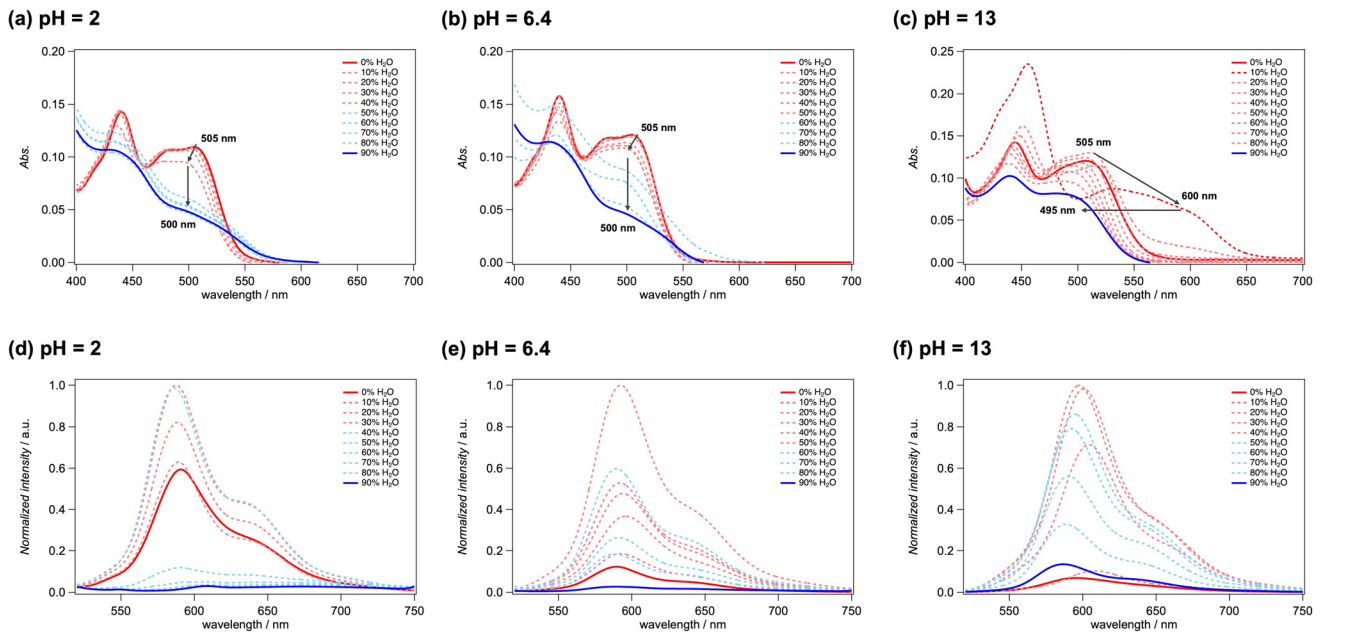

Fig. 6 (a)–(c) UV-vis spectra obtained from complex **1** in DMSO/H_2O mixtures having varying proportions of water. (d)–(f) Luminescence spectra for complex **1** in DMSO/H_2O mixtures with different water proportions. The pH of the H_2O was adjusted to 2.0, 6.4 or 13.0. Data were obtained with λ_{ex} = 505 nm and a complex concentration of 20 μM at 25 °C.

Table 1 Variations in the UV spectra of complex **1** with changes in pH

	pH = 2.0	pH = 6.4	pH = 13.0
Initial	505 nm	505 nm	505 nm
Red shift	—	—	105 nm
Blue shift	5 nm	5 nm	10 nm
$\Delta\lambda_{max}$	5 nm	5 nm	105 nm

$\Delta\lambda_{max}$ values. These data demonstrate a minimal peak shift of $\Delta\lambda_{max}$ = 5 nm across all acidic and neutral pH values. Conversely, a basic pH generated large red- and blue-shifts with a $\Delta\lambda_{max}$ of 105 nm. This was accompanied by aggregation or dispersion based on the specific proportion of water. That is, depending on the pH, water acted as a good or poor solvent for **1** so that the carboxy groups were protonated or deprotonated. This, in turn, modified the molecular assembly of the complex in solution leading to the spectral changes. In the case of complex **2**, similar spectral changes were observed (Fig. S6 and Table S4†). However, complex **3**, which had only one carboxy group at the top of the salophen ligand, was slightly more soluble in water. Thus, even under neutral conditions (pH = 6.4), a systematic peak shift was observed with variations in the water proportion (Fig. S7†). At the acidic pH, a sharp decrease in peak intensity based on the precipitation of **3** was seen, as also occurred with the other complexes, but a slight red-shift appeared in 90% water. This effect was possibly the result of colloid formation. The various peak shifts are presented in Table S5.†

Fig. 6d–f provide the normalised emission spectra of **1** in solutions with various water proportions and at different pH. At a pH of 2, the emission intensity increased on going to a 40% water proportion due to the higher local concentrations of the complex at the DMSO sites (Fig. 6d). That is, complex **1** exhibited AIEE phenomena in a good solvent (meaning DMSO).[34,35] However, the emission intensity was decreased significantly in solutions with more than 50% water as a consequence of the precipitation of **1** in response to acidification, which was consistent with the UV spectra. Similar behaviour was observed at a pH of 6.4 but the emission intensity gradually decreased because **1** was slightly soluble in neutral water (Fig. 6e). Under basic conditions (pH = 13.0) and with a 10% water proportion, the emission intensity increased slightly and λ_{em} was red-shifted from 590 to 620 nm. As mentioned, the deprotonated molecules were readily soluble in basic water, so oligomer formation occurred at water sites, which resulted in a red-shift in emission spectra. A blue-shift accompanied subsequent increases in the proportion of water, induced by the gradual dispersion of complex molecules and the loss of oligomer formation. The emission intensity decrease may also have partly resulted from thermal deactivation caused by the rotational motion of the carboxy groups. Complexes **2** and **3** showed similar trends with regard to luminescence characteristics. QYs of **1**–**3** in DMSO and DMSO–H_2O mixture are summarized in Table 2. As also can be understood from the luminescent measurements, QYs in all the complex increased in

Table 2 QYs (φ_{em}) of **1**–**3** in pure DMSO and DMSO–H_2O mixture

	DMSO	pH = 2.0	pH = 6.4	pH = 13.0
1	0.002[b]	0.002[b]	0.012[b]	0.026[a]
2	0.001[b]	0.001[b]	0.012[b]	0.015[b]
3	0.011[a]	0.015[b]	0.027[b]	0.037[a]

[a] Determined using the spectra showing the highest emission intensity in the DMSO–H_2O mixture. [b] Relatively determined based on absolutely obtained value.

mixture of DMSO and basic H_2O mixture, resulted in giving *ca.* 10-fold higher than mixing with acidic water.

For the practical use of such pH effect on the luminescence feature of the present platinum(II) complexes, the reversibility in spectroscopic changes with response to pH-adjusted water was studied. We measured luminescence spectra by consecutive addition of acid (2 M HCl) and base (2 M NaOH) to pure 20 μM DMSO solution of **1** (Fig. 7). In acidic solution of **1** adjusted by addition of 1 mL of 2 M HCl to the pure DMSO solution, strong emission that can be seen in naked eyes was not observed although slight emission peak was observed in spectroscopic measurements. This is because of complex molecules were diffused in DMSO site without molecular aggregation. On the other hand, purple emission was observed by addition of 2 mL of 2 M NaOH to the acidic solution wherein the solution became basic. This is attributed to the molecular aggregation in basic water site as good solvent, resulting in AIEE behaviour. That is, emission on/off behaviour that can be confirmed by naked eyes was observed between basic and acidic solution of **1**. To avoid the precipitation by addition of much water, the repeated experiment was conducted two times. This behaviour was also observed in **2** (Fig. S8a†). However, in case of **3**, only slight change was observed because of lower effect of the carboxy group at the top of salophen ligand on the emission behaviour based on molecular assembly change (Fig. S8b†).

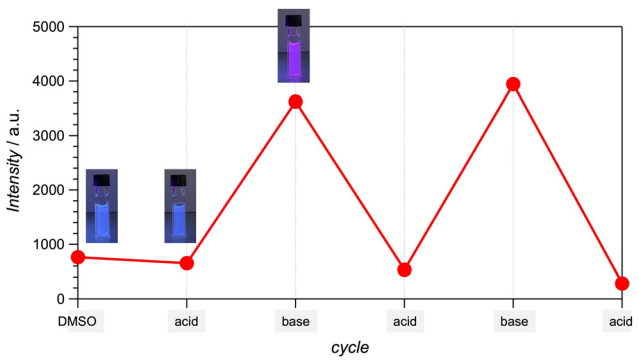

Fig. 7 Luminescence switching behaviour of complex **1** by addition of acid and base. 10 mL of 20 μM DMSO solution of **1** was consecutively diluted by acid (2 M HCl) and base (2 M NaOH).

Conclusions

We have reported carboxy-appended platinum(II) complexes that alter the protonation/deprotonation by organic acid/base addition, which influences on the luminescence spectra change. Furthermore, the present results reflect the protonation/deprotonation of carboxy substituents with changes of pH in water of its DMSO mixture, which in turn induce aggregation or repulsion in good solvent and lead to changes in UV-vis and luminescence spectra. Acidic and neutral pH conditions accelerate protonation of carboxy group, and the increasing of water proportion resulted in the loss of emission intensity due to the precipitation. On the other hand, basic pH condition caused the deprotonation of carboxy group, inducing AIEE phenomena efficiently. Based on these changes, complexes **1–3** each exhibit a peak shift with $\Delta\lambda_{max}$ = 95–105 nm in good solvent with aggregation or repulsion of molecules. Furthermore, emission on/off behaviour being confirmable in naked eyes were observed by addition of suitable acid and base. This study, which focuses on optical changes based on dynamic molecular assembly changes rather than the more common pH-induced resonance structural changes, provides new insights into the correlation between the luminescence properties of carboxy-appended molecular complexes and pH changes, and will contribute to the future construction of pH sensing devices based on molecular metal complexes.

Experimental

All reagents were used as received without further purification. Details of the procedures used to synthesize the carboxy-appended salophen ligand derivatives (**L1–L3**) are provided in the ESI.†

Synthesis of complexes 1–3

[Pt{(COOH)$_2$–salophen}] (1). **L-1** (0.121 g, 0.296 mmol), K_2CO_3 (0.122 g, 0.888 mmol) and K_2PtCl_4 (0.123 g, 0.296 mmol) were added to DMSO (3 mL) following which the mixture was stirred for 18 h at 80 °C. The resulting solution was added to water (50 mL) after which the complex was precipitated by adding 2 M HCl. This product was removed by filtration and washed with water, MeOH and ether to give complex **1** as an orange powder. Yield: 61.9%. ^{1}H-NMR (DMSO-d6): δ = 9.61 (s, 1H), 8.65–8.64 (d, 1H, J = 4.0 Hz), 8.45–8.41 (m, 1H), 8.05–8.02 (dd, 1H, J = 8.0 Hz), 7.48–7.44 (m, 1H), 7.14–7.12 (d, 1H, J = 8.0 Hz). Elemental analysis: calcd for $C_{22}H_{14}N_2O_6Pt{\cdot}2.5H_2O$ (642.48): C, 41.13; H, 2.98; N, 4.36. Found: C, 41.34; H, 3.18; N, 4.21. FAB-MS(−): m/z calcd for $[M - H]^-$: 596.5; found: 596.2.

[Pt{(COOH)$_3$–salophen}] (2). **L-2** (0.129 g, 0.296 mmol), K_2CO_3 (0.117 g, 0.888 mmol) and K_2PtCl_4 (0.120 g, 0.296 mmol) were added to DMSO (5 mL) after which the solution was stirred for 18 h at 80 °C. The resulting mixture was combined with water (50 mL) and 2 M HCl was added to precipitate the complex. The product was removed by filtration and washed with water, MeOH and ether to give complex **2** as an orange powder. The crude powder was dissolved in DMF and purified on a silica gel column to obtain complex **2**. Yield: 61.9%. ^{1}H-NMR (DMSO-d6): δ = 9.80 (s, 1H), 9.68 (s, 1H), 8.99 (s, 1H), 8.73 (d, 1H, J = 2.4 Hz), 8.62 (d, 1H, J = 2.4 Hz), 8.53–8.51 (d, 1H, J = 8.0 Hz), 8.04–7.98 (m, 2H), 7.92–7.89 (dd, 1H, J = 8.7 Hz), 7.11–7.07 (t, 2H, J = 8.0 Hz). Elemental analysis: calcd for $C_{26}H_{30}N_3O_{13.5}Pt{\cdot}4.5H_2O{\cdot}$DMF (642.48): C, 39.25; H, 3.80; N, 5.28. Found: C, 38.98; H, 3.48; N, 5.40. FAB-MS(−): m/z calcd for $[M - H]^-$: 640.4; found: 640.2.

[Pt{(COOH)–salophen}] (3). **L-3** (0.204 g, 0.566 mmol), K_2CO_3 (0.236 g, 1.71 mmol) and K_2PtCl_4 (0.234 g, 0.566 mmol) were added to DMSO (5 mL) after which the mixture was stirred for 18 h at 80 °C. The resulting solution was combined with water (50 mL) after which the complex was precipitated by adding 2 M HCl. The product was removed by filtration and then washed with water, MeOH and ether to give complex **3**. Yield: 75.7%. ^{1}H-NMR (DMSO-d6): δ = 9.69 (s, 1H), 9.63 (s, 1H), 8.99 (s, 1H), 8.55–8.53 (d, 1H, J = 8.0 Hz), 8.02–8.00 (d, 1H, J = 8.0 Hz), 7.98–7.96 (d, 1H, J = 8.0 Hz), 7.91–7.89 (d, 1H, J = 8.0 Hz), 7.64–7.57 (m, 2H), 7.15–7.14 (d, 1H, J = 4 Hz), 7.13–7.12 (d, 1H, J = 4.0 Hz), 6.84–6.78 (m, 2H). Elemental analysis: calcd for $C_{21}H_{14}N_2O_4Pt{\cdot}2H_2O$ (642.48): C, 42.79; H, 3.08; N, 4.75. Found; C, 42.73; H, 3.03; N, 4.63. FAB-MS(−): m/z calcd for $[M - H]^-$: 552.1; found: 552.1.

Author contributions

M. N. designed and supervised the project. S. F., N. I. and M. N. performed all lab experiments. S. F. and M. N. wrote the manuscript. T. K and H. Y. performed the DFT calculations. M. I. performed to measure the luminescence quantum yield. All authors contributed to the manuscript and have given approval to the final version.

Conflicts of interest

There are no conflicts to declare.

Acknowledgements

This work was supported by a JSPS KAKENHI Grant-in-Aid for Young Scientists (No. JP22K14695). M. N. also acknowledges financial support from the Tokuyama Science Foundation and Scholarship Fund for Young/Women Researchers.

References

1 H. Xu, R. Chen, Q. Sun, W. Lai, Q. Su, W. Huang and X. Liu, *Chem. Soc. Rev.*, 2014, **43**, 3259–3302.
2 V. W.-W. Yam, A. K.-W. Chan and E. Y.-H. Hong, *Nat. Rev. Chem.*, 2020, **4**, 528–541.

3 V. W.-W. Yam and Y.-H. Cheng, *Bull. Chem. Soc. Jpn.*, 2022, **95**, 846–854.
4 S. K. Fung, T. Zou, B. Cao, T. Chen, W. P. To, C. Yang, C. N. Lok and C. M. Che, *Nat. Commun.*, 2016, **7**, 10655.
5 A. S. Law, L. C. Lee, K. K. Lo and V. W. Yam, *J. Am. Chem. Soc.*, 2021, **143**, 5396–5405.
6 Y. Sun, Y. Lu, M. Bian, Z. Yang, X. Ma and W. Liu, *Eur. J. Med. Chem.*, 2021, **211**, 113098.
7 M. P. Coogan and V. Fernandez-Moreira, *Chem. Commun.*, 2014, **50**, 384–399.
8 Y. Zhang, T. S. Lee, J. M. Favale, D. C. Leary, J. L. Petersen, G. D. Scholes, F. N. Castellano and C. Milsmann, *Nat. Chem.*, 2020, **12**, 345–352.
9 J. Li and T. Chen, *Coord. Chem. Rev.*, 2020, **418**, 213355.
10 L. Zeng, S. Kuang, G. Li, C. Jin, L. Ji and H. Chao, *Chem. Commun.*, 2017, **53**, 1977–1980.
11 B. Higgins, B. A. DeGraff and J. N. Demas, *Inorg. Chem.*, 2005, **44**, 6662–6669.
12 N. Dey, D. Biswakarma and S. Bhattacharya, *ACS Sustainable Chem. Eng.*, 2018, **7**, 569–577.
13 L. C. Lee and K. K. Lo, *J. Am. Chem. Soc.*, 2022, **144**, 14420–14440.
14 R. Zhang and J. Yuan, *Acc. Chem. Res.*, 2020, **53**, 1316–1329.
15 D.-L. Ma, V. P.-Y. Ma, D. S.-H. Chan, K.-H. Leung, H.-Z. He and C.-H. Leung, *Coord. Chem. Rev.*, 2012, **256**, 3087–3113.
16 R. D. Costa, E. Orti, H. J. Bolink, F. Monti, G. Accorsi and N. Armaroli, *Angew. Chem., Int. Ed.*, 2012, **51**, 8178–8211.
17 R. C. Evans, P. Douglas and C. J. Winscom, *Coord. Chem. Rev.*, 2006, **250**, 2093–2126.
18 J. Garethwilliams, S. Develay, D. Rochester and L. Murphy, *Coord. Chem. Rev.*, 2008, **252**, 2596–2611.
19 F. Wei, S. L. Lai, S. Zhao, M. Ng, M. Y. Chan, V. W. Yam and K. M. Wong, *J. Am. Chem. Soc.*, 2019, **141**, 12863–12871.
20 V. W. Yam, V. K. Au and S. Y. Leung, *Chem. Rev.*, 2015, **115**, 7589–7728.
21 J. L. Tsai, T. Zou, J. Liu, T. Chen, A. O. Chan, C. Yang, C. N. Lok and C. M. Che, *Chem. Sci.*, 2015, **6**, 3823–3830.
22 D. Saito, T. Ogawa, M. Yoshida, J. Takayama, S. Hiura, A. Murayama, A. Kobayashi and M. Kato, *Angew. Chem., Int. Ed.*, 2020, **59**, 18723–18730.
23 M. Ebina, A. Kobayashi, T. Ogawa, M. Yoshida and M. Kato, *Inorg. Chem.*, 2015, **54**, 8878–8880.
24 B. C. Tzeng, B. S. Chen, C. K. Chen, Y. P. Chang, W. C. Tzeng, T. Y. Lin, G. H. Lee, P. T. Chou, Y. J. Fu and A. H. Chang, *Inorg. Chem.*, 2011, **50**, 5379–5388.
25 G. H. Sarova, N. A. Bokach, A. A. Fedorov, M. N. Berberan-Santos, V. Y. Kukushkin, M. Haukka, J. J. Frausto da Silva and A. J. Pombeiro, *Dalton Trans.*, 2006, 3798–3805, DOI: **10.1039/b602083f**.
26 M. Kato, *Bull. Chem. Soc. Jpn.*, 2007, **80**, 287–294.
27 H.-Q. Liu, T.-C. Cheung and C.-M. Che, *Chem. Commun.*, 1996, 1039–1040.
28 Y. Zhang, Z. Yin, F. Meng, J. Yu, C. You, S. Yang, H. Tan, W. Zhu and S. Su, *Org. Electron.*, 2017, **50**, 317–324.
29 W. Wu, J. Zhao, H. Guo, J. Sun, S. Ji and Z. Wang, *Chem. – Eur. J.*, 2012, **18**, 1961–1968.
30 A. Haque, L. Xu, R. A. Al-Balushi, M. K. Al-Suti, R. Ilmi, Z. Guo, M. S. Khan, W. Y. Wong and P. R. Raithby, *Chem. Soc. Rev.*, 2019, **48**, 5547–5563.
31 R. Kitaura, G. Onoyama, H. Sakamoto, R. Matsuda, S. Noro and S. Kitagawa, *Angew. Chem., Int. Ed.*, 2004, **43**, 2684–2687.
32 A. D. Becke, *J. Chem. Phys.*, 1993, **98**, 5648–5652.
33 M. J. Frisch, G. W. Trucks, H. B. Schlegel, G. E. Scuseria, M. A. Robb, J. R. Cheeseman, G. Scalmani, V. Barone, G. A. Petersson, H. Nakatsuji, X. Li, M. Caricato, A. V. Marenich, J. Bloino, B. G. Janesko, R. Gomperts, B. Mennucci, H. P. Hratchian, J. V. Ortiz, A. F. Izmaylov, J. L. Sonnenberg, D. Williams-Young, F. Ding, F. Lipparini, F. Egidi, J. Goings, B. Peng, A. Petrone, T. Henderson, D. Ranasinghe, V. G. Zakrzewski, J. Gao, N. Rega, G. Zheng, W. Liang, M. Hada, M. Ehara, K. Toyota, R. Fukuda, J. Hasegawa, M. Ishida, T. Nakajima, Y. Honda, O. Kitao, H. Nakai, T. Vreven, K. Throssell, J. A. Montgomery Jr., J. E. Peralta, F. Ogliaro, M. J. Bearpark, J. J. Heyd, E. N. Brothers, K. N. Kudin, V. N. Staroverov, T. A. Keith, R. Kobayashi, J. Normand, K. Raghavachari, A. P. Rendell, J. C. Burant, S. S. Iyengar, J. Tomasi, M. Cossi, J. M. Millam, M. Klene, C. Adamo, R. Cammi, J. W. Ochterski, R. L. Martin, K. Morokuma, O. Farkas, J. B. Foresman and D. J. Fox, *Gaussian 16, Revision C.01*, Gaussian, Inc. Wallingford CT, 2016.
34 B. K. An, S. K. Kwon, S. D. Jung and S. Y. Park, *J. Am. Chem. Soc.*, 2002, **124**, 14410–14415.
35 V. Sathish, A. Ramdass, P. Thanasekaran, K.-L. Lu and S. Rajagopal, *J. Photochem. Photobiol., C*, 2015, **23**, 25–44.